

## Visible and Near-Infrared Contrast of Faculae in Active Region NOAA 8518 \*

Yan Xu, Guo Yang, Jiong Qiu, Tom J. Spirock, Ju Jing, Carsten Denker and Haimin Wang

Center for Solar-Terrestrial Research, New Jersey Institute of Technology 323 Martin Luther King Blvd, Newark, NJ 07102, USA; yx2@njit.edu

Received 2004 May 28; accepted 2004 July 12

**Abstract** We compare the contrast of faculae, in visible light and in the near-infrared (NIR), that were associated with the active region NOAA 8518 which crossed the solar disk from April 19 to 27, 1999. We obtained NIR continuum images at  $1.6\ \mu\text{m}$  at the Big Bear Solar Observatory (BBSO) with an Indium Gallium Arsenide (In Ga As) NIR digital camera. We also obtained high-resolution longitudinal magnetograms and visible light filtergrams at  $610.3\ \text{nm}$  with the newly developed Digital Vector Magnetograph (DVMG). Our data show that the contrast of faculae has the same sign in both the visible and the NIR. We did not find any so-called “dark faculae”, faculae that are bright in the visible and simultaneously dark in the NIR. We determined a threshold magnetic flux density that separates pores from faculae.

**Key words:** Sun: infrared — Sun: faculae

### 1 INTRODUCTION

Faculae are small-scale brightenings in the photosphere of the Sun and are usually associated with chromospheric plages. It is generally believed that these photospheric bright points are related to small-scale magnetic features and more than 90% of the magnetic flux outside sunspots is concentrated in small tubes (Keller 1992; Zhang 1998). These flux-tubes contribute to the observed changes in the solar irradiance of the Sun over the 11-year activity cycle (Foukal & Lean 1988; Schatten 1988; Kuhn 1988). Several competing flux-tube models try to explain the structure of the faculae. The “hot wall” model (Spruit 1976) considers the faculae as small flux-tubes with diameters of about 100 km. When observed near the center of the solar disk, one can see deep into the photosphere due to the low opacity of the photospheric material inside the flux-tube. The vertical, hot, bright walls are not visible. Therefore, the contrast of the faculae will be very low when observed at this location. When observed at moderate heliocentric angles ( $> 60^\circ$ ) the hot wall of the faculae, which is brighter than the average surrounding photosphere, becomes visible and the contrast increases. When observed at extreme heliocentric angles ( $> 80^\circ$ ), the side of the flux-tube that is closer to the center of the solar disk blocks

---

\* Supported by the National Natural Science Foundation of China.

the visible hot wall and the contrast decreases. The second model attempting to explain the faculae is the “hot cloud” model (Chapman 1979). This model assumes that faculae are formed by magnetic heating. The contrast of the facula would monotonically increase as it moves from the solar disk center to the limb and the apparent thickness of the hot cloud increases due to the change in the apparent geometry. The third model is the “hillock” model (Schatten 1986), which is very similar to the hot cloud model, where faculae are considered to be hot plasma emitted by flux-tubes around sunspots. Observation in the near infrared (NIR) can provide additional clues about the structure of the faculae, because the opacity of the solar atmosphere is minimum at  $1.6\ \mu\text{m}$ . Several authors have already studied the properties of faculae with NIR observations (Foukal 1989; Foukal 1990; Moran 1992; Foukal 1994; Wang 1987; Wang 1998). Thus far, most observations have favored the hot wall model.

Foukal and colleagues first reported dark faculae near the solar disk center (Foukal 1989) and, subsequently, published several papers describing their work in greater detail (Foukal 1990; Foukal 1991; Foukal 1994). In these papers, dark faculae are defined as facular regions that are bright at  $\text{Ca K}+0.38\ \text{\AA}$  but tend to be darker than the quiet photosphere in IR, even when they do not contain any spots detectable in the visible continuum (Foukal 1989). They conclude that these dark features are caused by a layer of hot plasma that becomes transparent at  $1.63\ \mu\text{m}$ . Schatten et al. (1991) performed similar work using the hillock model. Sobotka et al. (2000) proposed a new definition of dark faculae. Their data were taken in the infrared bands at  $0.8\ \mu\text{m}$  and  $1.55\ \mu\text{m}$ . The contrast at  $1.55\ \mu\text{m}$  is always lower than the contrast at  $0.8\ \mu\text{m}$ . In order to make the images in the two different bands comparable, they multiply the contrast images at  $1.55\ \mu\text{m}$  by a constant, which would make the granular contrast to be the same at  $0.8\ \mu\text{m}$  and  $1.55\ \mu\text{m}$ . They define dark faculae as structures that are dark in the difference image between the  $0.8\ \mu\text{m}$  and the reduced  $1.55\ \mu\text{m}$  images. They assumed that dark faculae are a new type of solar feature with characteristics between the faculae and the pores. Cuberes (2002) extended Sobotka et al.’s work by using high resolution images. They found that faculae have negative differential contrasts when  $\mu > 0.6$  ( $\mu = \cos\theta$ ,  $\mu = 1$  for the disk center and  $= 0$  for the limb). Their results also showed that the dark faculae always appear around the pores. In our observations, we use an InGaAs NIR camera to observe the contrast at  $1.56\ \mu\text{m}$  and the DVMG system to obtain high resolution longitudinal magnetograms. Our preliminary results were presented in a workshop proceedings (Xu 2002). As we will demonstrate below, our data show that there are no dark faculae if we use original definition of dark faculae by Foukal. We conclude that the dark structures previously thought to be dark faculae are simply pores that were probably unresolved in the previous observations. Much of the discussion of the existence of dark faculae is merely a question of proper photometric definition. In addition, we find a critical value of magnetic flux density which divides the faculae and the pores: if the flux density is below this critical value, then the flux-tubes appear as faculae; if the flux density is above, then a pore.

## 2 OBSERVATION

We observed the active region NOAA 8518 at BBSO as it crossed the solar disk from April 19 to 27, 1999. It was a simple, decaying  $\alpha$ -sunspot without much activity. The series of NIR image are shown in Fig. 1. We can see some basic properties of this active region in these pictures, including the gradual disappearance of the pores east of the sunspots. The images taken on April 20 and 21 are closer to the disk center than others. Figure 2 shows the continuous

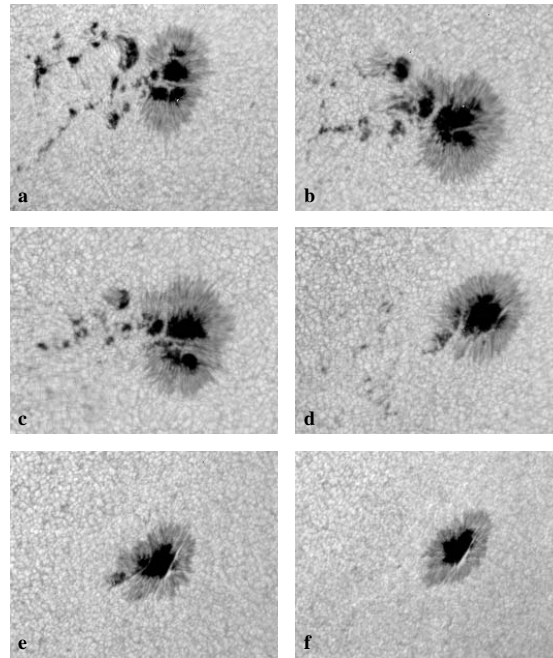


Fig. 1 NIR images of active region NOAA 8518 observed in April, 1999. (a) April 19, (b) April 20, (c) April 21, (d) April 25, (e) April 26, (f) April 27.

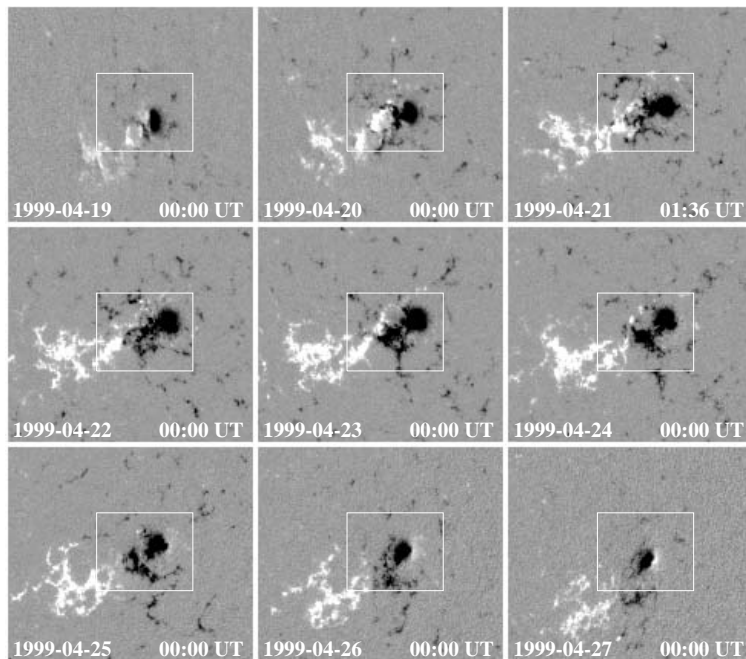


Fig. 2 MDI magnetograms taken from April 19 to 27, 1999. The white box shows the field of view of the IR images in Figure 1. The magnetograms are scaled between  $-400$  G and  $+250$  G.

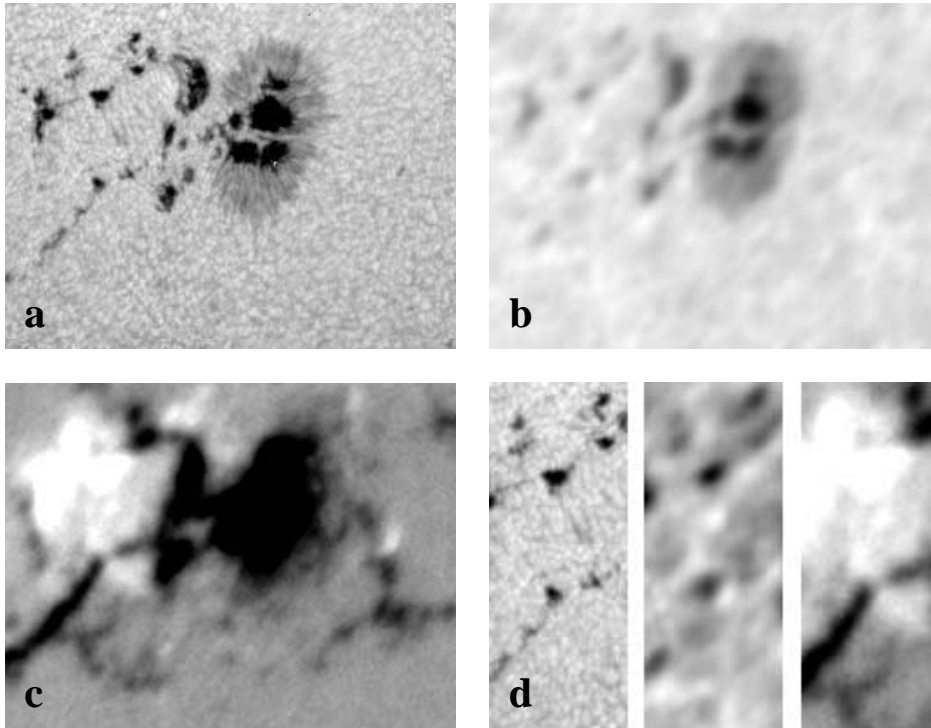


Fig. 3 Images of active region NOAA 8518 at different wavelengths observed on April 19, 1999. (a) NIR filtergram, (b) visible light filtergram, (c) magnetogram, and (d) sub-frames from (a), (b), and (c) on the region of interest. The magnetograms are scaled between  $-400$  G and  $+250$  G.

MDI magnetograms of the active region from April 19 to 27, 1999. A compiled movie shows that many small flux-elements of opposite polarity are cancelling each other out locally. In a separate study, we will study the energy dissipation of these cancelling magnetic features.

Two types of time sequences were obtained during the observation. The DVMG system at the 25 cm vacuum refractor obtained longitudinal magnetograms and intensity maps while the InGaAs camera obtained NIR filtergrams at the 65 cm vacuum reflector. The DVMG system uses two nematic liquid crystal variable retarders and the retardance can be changed by means of an applied voltage to select the desired polarization state. A ferroelectric liquid crystal is used as a  $1/2 \lambda$  plate and its fast axis can be rotated by means of an applied voltage. The ferroelectric crystal is used along with a fixed linear polarizer to select either the Stokes-( $I+V$ ) or Stokes-( $I-V$ ) component of the magnetic field. The observations are made in the wing of the magnetically sensitive Ca I absorption line at 610.3 nm with a 0.025 nm bandwidth Zeiss filter. A  $1024 \times 1024$  pixel CCD camera (manufacture Design Silicon Mountain) is used in the  $2 \times 2$  binning mode, which yields an image scale of  $0.6'' \text{ pixel}^{-1}$ . For this study, only longitudinal magnetograms were obtained (Stokes- $V/I$ ). We used Kitt Peak full disk magnetogram data to determine the calibration function  $C(\rho)$ , which converts the degree of polarization  $\rho$  into magnetic flux density measured in Gauss. The calibration procedure is given in Xu (2002). The result is 1% polarization  $\approx 230$  Gauss for each degree of polarization. An example of a magnetogram is shown in Fig. 3c. A selected frame of short-exposure image in the line wing

of the Ca I 610.3 nm absorption line is defined as the “white-light” image. Since the Ca I line is rather weak, we use this line wing image as a proxy of the continuum (origin higher in the photosphere). An example of the white light image is shown in Fig. 3b. The InGaAs NIR camera has a sensitivity range from  $0.9\ \mu\text{m}$  to  $1.7\ \mu\text{m}$  with quantum efficiency greater than 75% from  $1.0\ \mu\text{m}$  to  $1.6\ \mu\text{m}$ . The optics were set up to produce an image scale of  $0.3''\ \text{pixel}^{-1}$ . A custom made interference filter centered at  $1.56\ \mu\text{m}$  with a pass band of 4 nm was used to select the wavelength range. The exposure time was 0.1 ms. Figure 3a shows an example of NIR image after the dark and flat field frame corrections.

### 3 DATA ANALYSIS

In this analysis, we use the data obtained on the three days of best seeing, April 19, 20, and 25. Due to the fact that the field-of-view (FOV) of the NIR camera was much smaller than that of the visible-light camera, we needed to align the images and restrict the data analysis to the common FOV. In addition, the image scales had to be matched by re-sampling the “low resolution” magnetogram and white-light data to the image scale of the NIR observations. The NIR filtergram, white light image, and magnetogram of a selected region can be seen in Fig. 3d. We selected this particular region because it avoids the main sunspot while still contains strong plage features.

#### 3.1 Visible Contrast as a Function of NIR Contrast

To measure the contrast of the faculae in the visible as a function of that in the NIR, we selected the area near NOAA 8518 shown in Fig. 3d. We plotted the visible contrast as a function of the NIR contrast as scatter diagrams (Figs. 4a, 4c, and 4e for April 19, 20, and 25, respectively). The contrast value is positive or negative according as the object is brighter or darker than the mean photospheric intensity in the region. The correlation between the visible and NIR contrasts can be seen more clearly in the averaged plots in Figs. 4b, 4d, and 4f, averaged over the columns of Figs. 4a, 4c, and 4e. The vertical line at each point indicates the standard deviation. These correlation plots show that if a particular area is dark in the visible, then it is also dark in the NIR. We find no faculae that are bright in the visible but dark in the NIR.

In addition, we did similar analyses to those of Sobotka et al. (2000) and Cuberes (2002), with the difference that we used the images at  $0.61\ \mu\text{m}$  instead of  $0.8\ \mu\text{m}$ . Our difference images also show some dark features. However, two points should be made here. First, under the new definition, if a feature has positive contrast both at  $1.55\ \mu\text{m}$  and  $0.61\ \mu\text{m}$ , it may still be regarded as a dark facular if it has a negative value in the difference image, that is, if it has a lower contrast in  $1.55\ \mu\text{m}$  than in  $0.6\ \mu\text{m}$ . Second, our results show that most of the dark faculae according to the new definition are around pores. This result agrees with Sobotka et al. (2000) and Cuberes 2002. But this dark ring could be caused by artefacts, such as mis-alignment or mis-scaling of the images at the two wavelengths.

#### 3.2 Threshold of Magnetic Flux Density

We also studied the magnetic properties of the NIR features by aligning the visible-light images, NIR filtergrams and Ca I magnetograms, using the same procedure as for aligning the visible-light images and NIR filtergrams. Due to the limited resolution of the magnetograms, we can only measure the mean magnetic flux density rather than the actual field strength.

We now discuss the threshold of magnetic flux density. We plotted the flux density as a

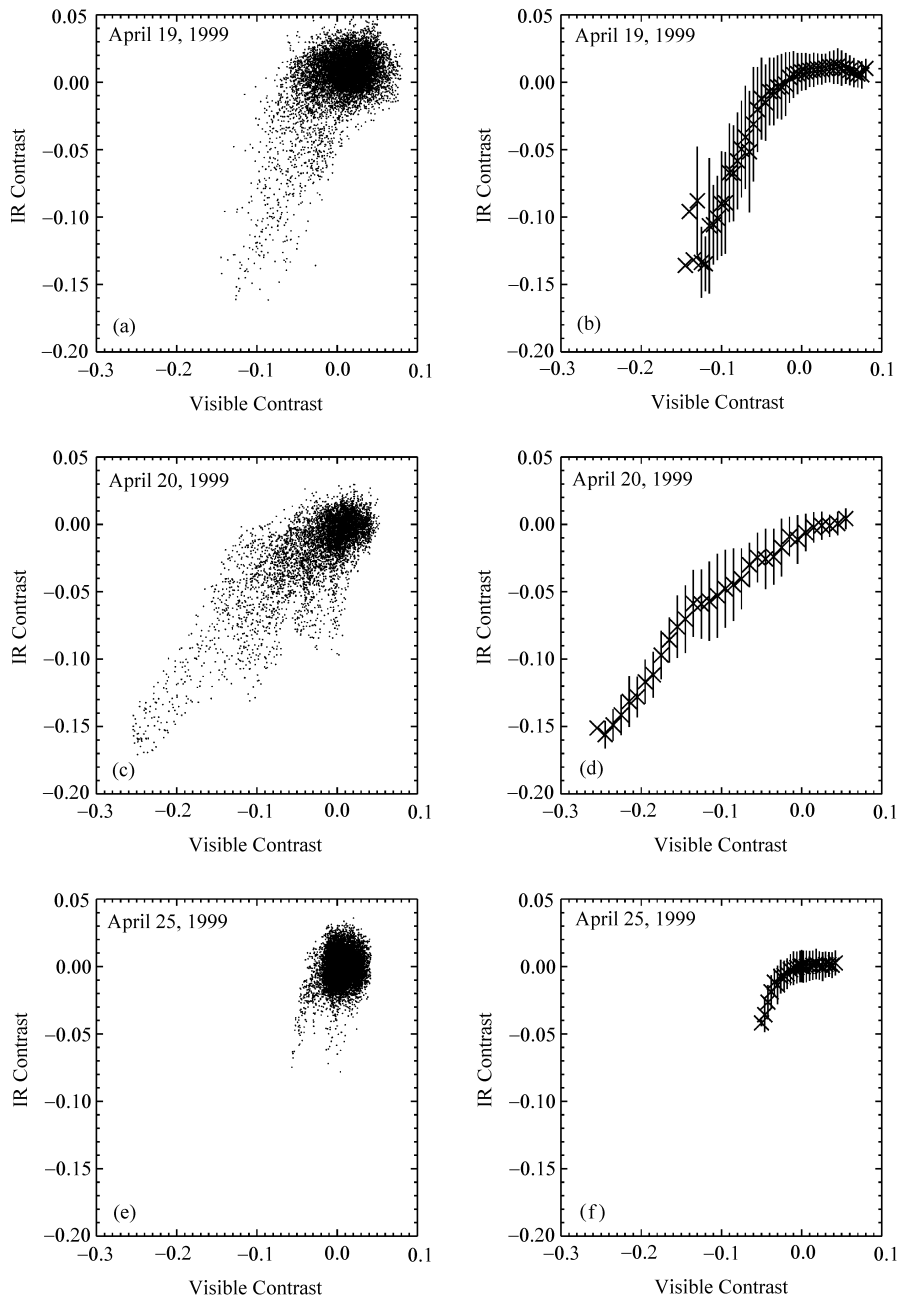


Fig. 4 Panels (a), (c), and (e) show the scatter plots for the visible contrast as a function of the NIR contrast, and (b), (d), and (f) show the averaged plots.

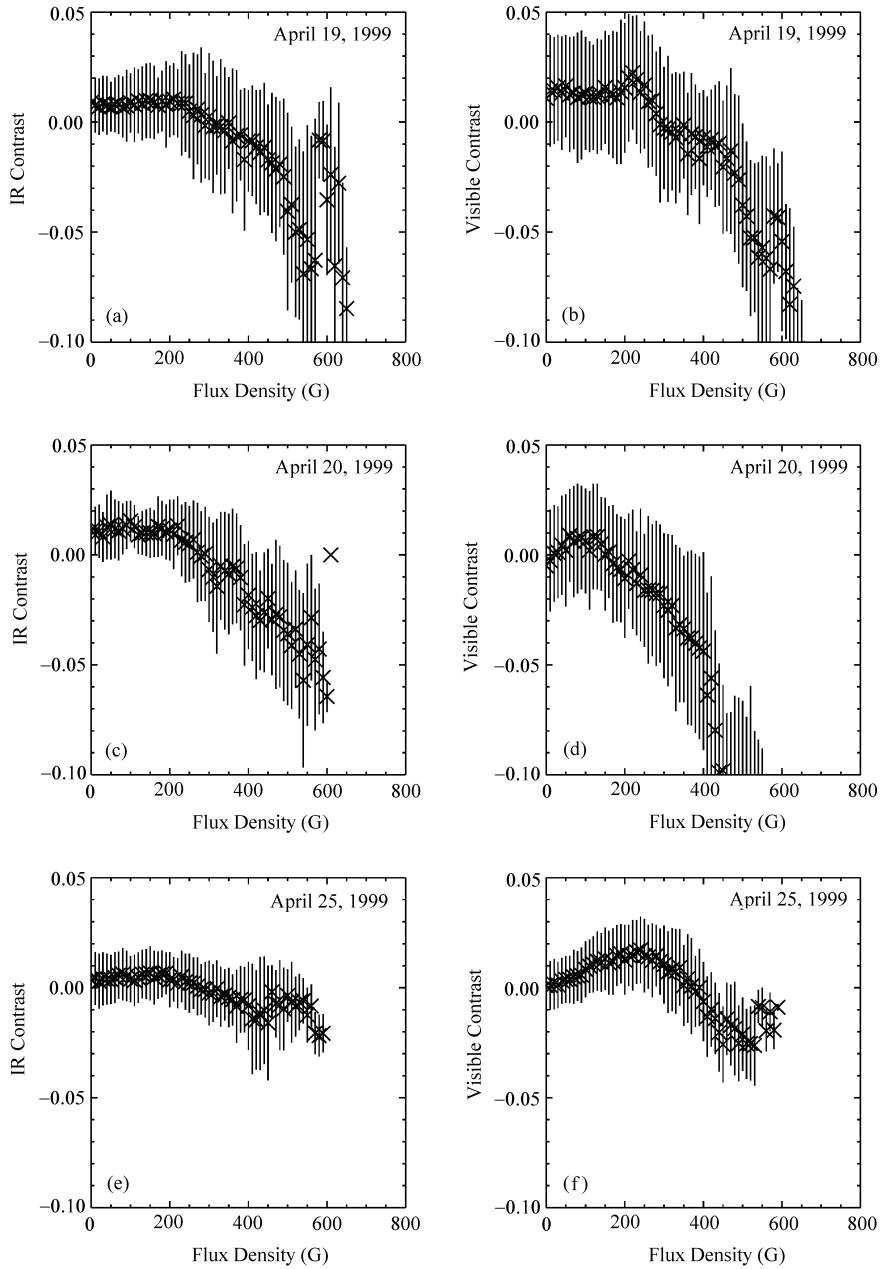


Fig. 5 Panels (a), (c), and (e) plot the NIR contrast as a function of the magnetic flux density, and (b), (d), and (f) plot the visible contrast as a function of the magnetic flux density.

function of the NIR contrast in Figs. 5a, 5c, and 5e for April 19, 20, and 25, respectively. We also plotted the flux density as a function of the visible contrast in Figs. 5b, 5d and 5f for the same dates. As can be seen in these plots, each curve can be divided into two parts, a part at the lower flux densities which exhibits a small slope, the contrast not changing rapidly with increasing flux density, and a part where, as the magnetic flux density increases, the slope begins to increase and the contrast changes much more rapidly. This typically occurs around 200–250 G. The two parts of the curve represent different features with different relationships between the contrast and the magnetic field strength.

We fit both parts of each curve separately by a straight line and define the intersection of the two lines as the “magnetic threshold” that separates faculae and pores. The threshold values for both the visible and the NIR are given in Table 1. Please note the thresholds are thresholds in the flux density and not in the field strength. The average value of the threshold is approximately 220 G. This value can be translated into a flux per resolution element of the order of  $10^{17}$  Mx, and value agrees with the results of Moran (1992), Zirin (1992), and Wang (1998). Our results also show that the negative contrast increases with the flux density (Moran 1992).

**Table 1** Magnetic Threshold Values

Date	$\mu$	NIR	Visible
April 19, 1999	0.72	$220 \pm 20$ G	$210 \pm 20$ G
April 20, 1999	0.82	$210 \pm 20$ G	$190 \pm 20$ G
April 25, 1999	0.85	$230 \pm 20$ G	$230 \pm 20$ G

#### 4 CONCLUSIONS

Our data show that the contrast of dark features at  $1.56 \mu\text{m}$  is less than the contrast at  $610.3 \text{ nm}$ . This is not surprising for any features that follow Planck’s radiation law. We also find that the contrast of faculae has the same sign in both the visible and NIR. Therefore, there is no evidence in our study for the existence of dark faculae according to the original definition of Foukal et al. We find that what has been previously thought to be dark faculae are actually pores. Our observations were obtained at  $1.56 \mu\text{m}$  whereas Foukal used  $1.63 \mu\text{m}$ . However, such a difference in wavelength should not be the cause for the different results because the height of formation at the two wavelengths differs by less than 5 km, which is insignificant (Wang 1998). We believe that the different results arise due to the fact that Foukal was actually observing unresolved pores which were mistaken to be dark faculae. In addition, the dark faculae defined by Sobotka and Cuberes are not the same as the dark faculae in Foukal’s original definition. Another result we obtained is the determination of a threshold magnetic flux density that separates faculae from pores. Our data show that this threshold is between 200 G and 250 G.

**Acknowledgements** We would like to thank the referee and Dr. Jingxiu Wang for valuable comments. We are grateful to the BBSO observing staff for their support in obtaining the data. This work is supported by NSF under grants ATM-0076602, ATM-0086999, ATM-0236945, NASA under grants NAG5-9682, NAG5-9501, and NAG5-10910, by NSFC-10103004, and by Chinese NSF through 2001A0027Q.

## References

- Chapman G., 1979, *ApJ*, 232, 923
- Cuberes M., Vázquez M., Bonet J. A., Sobotka M., 2002, *ApJ*, 570, 886
- Foukal P., Lean J., 1988, *ApJ*, 38, 347
- Foukal P., Little R., Mooney J., 1989, *ApJ*, 336, L33
- Foukal P., Little R., Graves J., Rabin D., Lynch D., 1990, *ApJ*, 353, 712
- Foukal P., Harvey K., Hill F., 1991, *ApJ*, 383, L89
- Foukal P. Moran T., 1994, In: D. Rabin et al. eds., *Infrared Solar Physics*, World Scientific, p.23
- Keller C. U., 1992, *Nature*, 359, 307
- Kuhn J., Libbrecht K., Dicke R., 1988, *Science*, 242, 908
- Moran T., Foukal P., Rabin D., 1992, *Solar Phys.*, 142, 35
- Schatten K., Mayr H., Omidvar K., Maier E., 1986, *ApJ*, 311, 460
- Schatten K., 1988, *Geophys. Res. Lett.*, 15, 121
- Schatten K., Mayr G., 1991, *ApJ*, 372, 728
- Sobotka M., Vazquez M., Cuberes M., Bonet J. A., 2000, *ApJ*, 544, 1155
- Spruit H. C., 1976, *Solar Phys.*, 50, 269
- Wang H., Zirin H., 1987, *Solar Phys.*, 110, 281
- Wang H., Spirock T. J., Goode P. R., Lee C., Zirin H., 1998, *ApJ*, 495, 957
- Xu Y., Wang H., Denker C., Yang G., Spirock T. J., Qiu J., 2002, *ASP Conf. Ser.*, 286, 201
- Zhang H., Scharmer G., Lofdahl M., Yi Z., 1998, *Solar Phys.*, 183, 283
- Zirin H., Wang H., 1992, *ApJ*, 385, L27